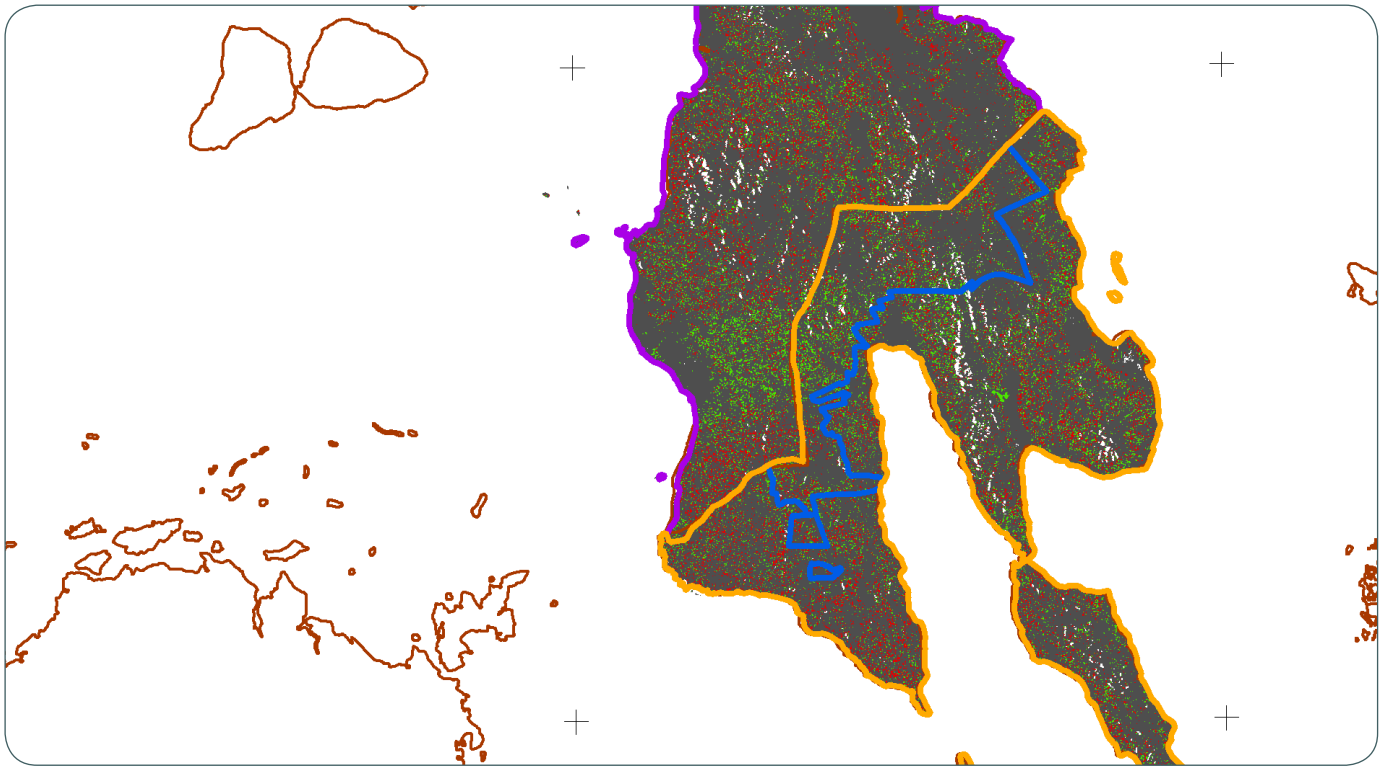

Landsat Land Cover Classification of Leyte, Island, Eastern Visayas, Philippines

Support to processing of remote sensing data for the establishment of a pilot MRV system for REDD+ on Leyte Island

giz Deutsche Gesellschaft für Internationale Zusammenarbeit (GIZ) GmbH

On behalf of

Federal Ministry for the Environment, Nature Conservation and Nuclear Safety

of the Federal Republic of Germany

Imprint

This publication is by the Deutsche Gesellschaft für Internationale Zusammenarbeit through the National REDD+ System Philippines Project, funded by the German Federal Ministry for the Environment, Nature Conservation and Nuclear Safety (BMU) under its International Climate Initiative. The BMU supports this Initiative based on a decision of the German Parliament. For more information, see http://www.international-climate-initiative.com.

As a federally owned enterprise, GIZ supports the German Government in achieving its objectives in the field of international cooperation for sustainable development.

Items from named contributors do not necessarily reflect the views of the publisher.

Published by
Deutsche Gesellschaft für Internationale Zusammenarbeit (GIZ) GmbH

Registered offices
Bonn and Eschborn, Germany
T +49 228 44 60-0 (Bonn)
T +49 61 96 79-0 (Eschborn)

Responsible
Dr. Bernd-Markus Liss
Principal Advisor
National REDD+ System Philippines
E: bernd-markus.liss@giz.de

Department of Environment and Natural Resources
Climate Change Office, 2nd Floor, FASPO Building
Visayas Avenue, Quezon City, 1101 Philippines

T: +63 2 929 6626 local 207
F: +63 2 829 3374

Author
John Truckenbrodt

Editors
Mari Trix Estomata, F. Mara Mendoza

Layout / Design
F. Mara Mendoza

Printed and distributed by
Deutsche Gesellschaft für Internationale Zusammenarbeit (GIZ) GmbH

Place and date of publication
Manila, Philippines
October 2013

Landsat Land Cover Classification of Leyte, Island, Eastern Visayas, Philippines

Support to processing of remote sensing data for the establishment of a pilot MRV system for REDD+ on Leyte Island

Table of contents

Abstract

With the objective of estimating the remaining forest cover on Leyte Island, land cover classifications using Landsat 4 TM, Landsat 5 TM and Landsat 7 ETM+ were performed for the years 1989, 1994, 1996 and 2001. In order to reduce cloud cover and shadow obstruction, a total of 37 images were processed and then fused together. A Support Vector Machine (SVM) was chosen as classifier. The accuracy for the classified images was above 80% for each image. A total of about 66,000 hectares were detected as deforested in the time frame from 1989 to 2001.

1 Introduction

During the United Nations Framework Convention on Climate Change (UNFCCC) Conference of the Parties (COP) 13 in Bali on December 2007, the international community has called upon countries to explore the concept of reducing emissions from deforestation and forest degradation (REDD) as a new mechanism to combine forest protection with objectives of climate protection, biodiversity conservation and improvement of local livelihoods. The project "Climate-relevant Modernization of Forest Policy and Piloting of REDD Measures in the Philippines," funded under the International Climate Initiative of the German Federal Ministry for the Environment, Nature Conservation and Nuclear Safety (BMU) supports the country's efforts toward forest and climate protection, and the development of appropriate policy and instruments. The successor project "National REDD+ System Philippines" is supporting the scaling up of technical solutions toward a national system for measuring, reporting and verification (MRV) of REDD+ results. The present study has been prepared during an internship with the Deutsche Gesellschaft für Internationale Zusammenarbeit (GIZ) GmbH at the Philippine's Department of Environment and Natural Resources (DENR) under the National REDD+ System Project from March to September 2013.

In discussion with DENR, Leyte Island, situated in the Eastern Visayas region of the Philippines, had been selected in 2009 as a site for piloting of REDD+ measures under the Philippine National REDD-Plus Strategy (PNRPS). The current processing of multispectral optical data and radar data to detect deforestation patterns in the pilot site (see Estomata, 2013a, 2013b) needs to be integrated into a consistent workflow covering multiple reporting periods (GIZ, 2012). This will inform a forest and land use change assessment for the establishment of data on preparing reference and reference emission levels for REDD+ implementation at a sub-national level, i.e. Leyte Island.

The Landsat classification performed in this study is part of this effort to achieve highest possible temporal coverage of satellite images for the island and quantify land cover and use changes. It can therefore be seen in conjunction with the forest resources assessment (FRA) on Leyte Island (DfS Deutsche Forstservice GmbH, 2013) for elaboration of an internationally compliant system for REDD MRV as outlined in the conceptual approach to REDD+ MRV in the Philippines (Seifert-Granzin, 2013).

A total of 37 images from 1989 to 2001 were acquired from the United States Geological Survey (USGS). The image preprocessing consisted of the following major steps: calibration, atmospheric correction and cloud/-shadow masking, radiometric normalization, terrain correction and image fusion. Subsequently, a Support Vector Machine (SVM) Classification was performed to delineate forest vegetation, non-forest vegetation and urban area/bare soil. Finally, all four classification results were compared in order to detect deforestation. **Figure 1** displays a visualization of the pursued workflow. Further description on the integrated data products and the single processing steps is given in the following chapters.

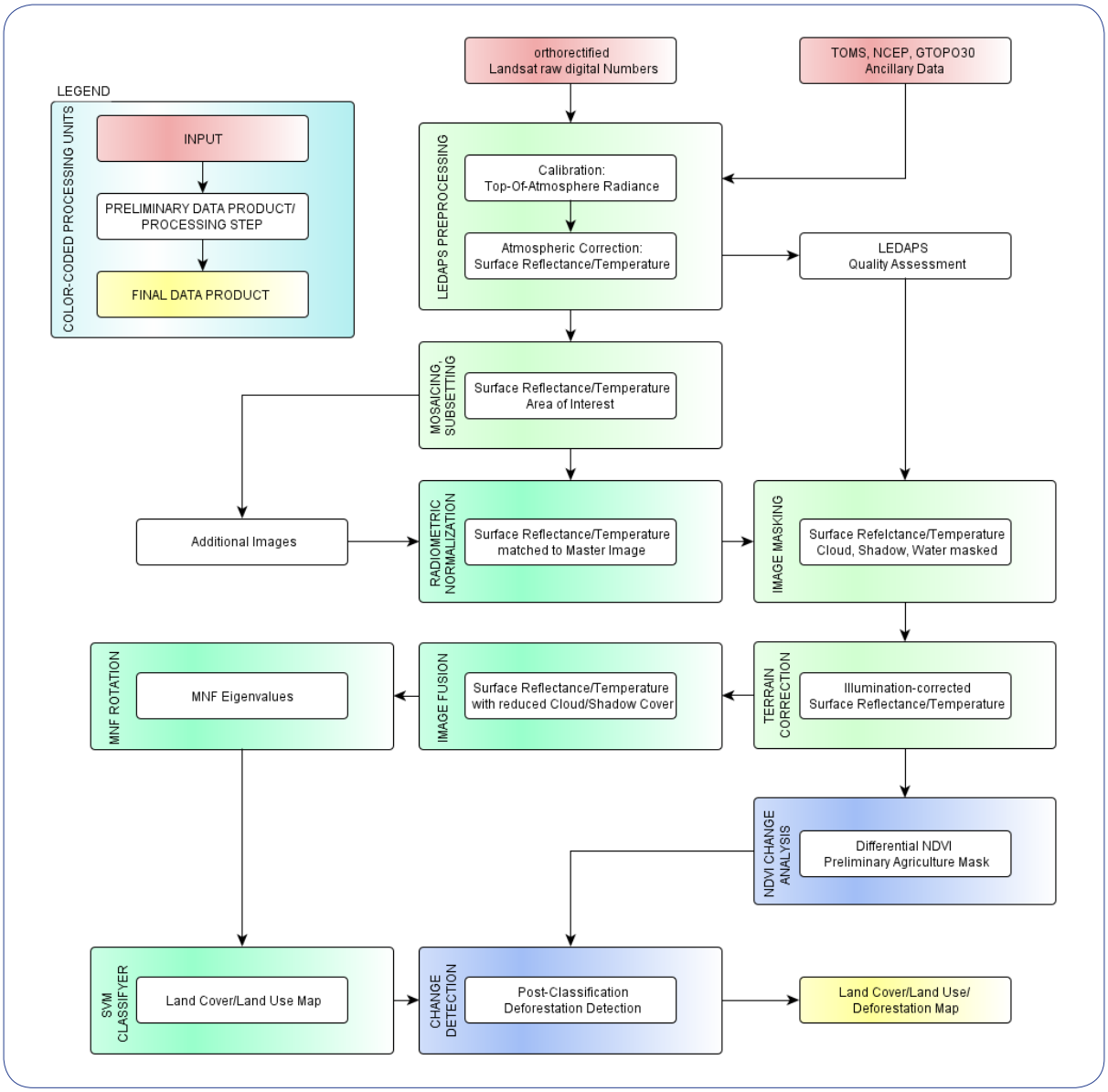

Figure 1. Visualization of the image processing workflow

Green boxes represent single image preprocessing; turquoise boxes represent processing steps incorporating several images combined to reduce cloud coverage; blue box processing steps incorporate multiple cloud-reduced image mosaics from different acquisition years for change detection.

1.1 Study Area

The island of Leyte is located in the Eastern Visayas region of the Philippines with center coordinates of 10°47'38" N 124°48'39" E. It expands approximately 170 km from north to south and 100 km west to east, covering an area of about 7,368 km2. Predominant land use is coconut tree plantation with trees present as pure plantations but, more commonly, as single trees in forested areas in different proportions. The island is traversed by a mountain range with peaks up to 578 m high.

1.2 Data

For classification and change detection, a total of 37 images of sensors Landsat-4 Thematic Mapper (TM), Landsat-5 TM and Landsat-7 Enhanced Thematic Mapper (ETM+) were used, which are freely available via the Earth Explorer service of the United States Geological Service (USGS). See Tab. 8 for a full list of all images.

These images were integrated to produce four cloud-reduced mosaics, which incorporate the time steps 1989–90, 1993–94, 1995–96 and 2000–01.

For atmospheric correction (see Section 2.2 for details), additional data products were included to enhance modeling of spatial heterogeneity of the atmosphere. A brief description is given in the following.

Ozone concentration measurements of the Total Ozone Mapping Spectrometer (TOMS), onboard the satellite Earth Probe, were included. This sensor estimates the optical depth (transparency) of the atmosphere by correlating measured radiance of different ultraviolet wavelengths. Due to their different atmosphere interaction characteristics, ozone absorption in particular, a lesser portion of the sun's energy is transmitted through the atmosphere and reflected back to be perceived by the sensor. This is then compared to direct measurements of sun's radiance (solar irradiance). A 90% daily coverage was achieved with a geometrical resolution of 1.25° longitude and 1.00° latitude (McPeters et al. 1998:3,13; Masek et al. 2006:69). Refer to McPeters et al. (1998) for comprehensive TOMS sensor and algorithm descriptions.

Also integrated were the surface pressure and precipitable water (water vapor), both of which are NCEP/NCAR Global Reanalysis Products that are synergistic multi-data products offered by the US National Center for Environmental Prediction (NCEP) and National Center for Atmospheric Research (NCAR). NCEP is part of the National Oceanic and Atmospheric Administration (NOAA) National Weather Service (NWS) (NCEP/NCAR 2001). Within this, data from surface measurements, radiosonde, aircraft and satellite are assimilated together with supporting modeling approaches (Kistler et al. 2001).

Also, Digital Elevation Model (DEM) GTOPO30 was included. This multi-source dataset with a geometric resolution of 30 arc seconds (1 km) was produced in 1996 as a joint effort of several international organizations coordinated by the US Geological Survey's Center for Earth Resources Observation and Science (USGS EROS). See USGS EROS (2012) for reference.

2 Image Preprocessing

In order to combine several images acquired on different dates throughout the year, great care needs to be taken in radiometrically matching the different acquisitions. The preprocessing steps include calibration (conversion of image digital numbers to top-of-atmosphere [TOA] radiance), atmospheric correction (conversion of TOA radiance to surface reflectance [SR]), cloud and cloud shadow masking, radiometric normalization, terrain correction and, finally, image stitching. These steps, including the necessary scientific terms, will briefly be described in the following. All steps, except preliminary image mosaicking and clipping as well as the final image stitching, have been performed with the Landsat Ecosystem Disturbance Adaptive Processing System (LEDAPS) software (Masek et al. 2013). The open source code is freely available via the Oak Ridge National Laboratory (ORNL) Distributed Active Archive Center for biochemical dynamics (DAAC), which is part of the National Aeronautics and Space Administration (NASA) Earth Observing System Data and Information System (EOSDIS) (Masek et al. 2013).

2.1 Calibration

The conversion of the raw image's unit less digital numbers into at-sensor radiance (ASR) in W*m-2*sr-1*µm-1 (Watts per square meter per steradian per micrometer) is calculated by using calibration factors included in a metadata text file, which is delivered together with the actual image data of Landsat (NASA 2011:117). Further, optical ASR is corrected for solar zenith (incidence angle of the Sun's radiation approaching the atmosphere), Sun–Earth distance (mainly depending on the day of year) and solar irradiance (solar radiance approaching the Earth, W*m–2) to acquire TOA reflectance (Masek et al. 2006:69). TOA reflectance, also referred to as planetary reflectance of albedo, is given in percent. Band 6 thermal radiance is converted to effective at-satellite temperature (thermal energy exiting the atmosphere expressed in Kelvin; thermal energy: electromagnetic radiation with wavelengths of 3–15 µm) using the calibration factors recommended in the Landsat Science Data Users Handbook (NASA 2011:120).

2.2 Atmospheric Correction

The conversion of TOA reflectance to surface reflectance consisted of the following steps: extraction of aerosol optical thickness (AOT) with the dark, dense vegetation method (DDV) (Kaufman et al. 1997) and then supplying it to a Second Simulation of the Satellite Signal in the Solar Spectrum (6S) radiative transfer algorithm together with the TOMS ozone, GTopo30 DEM, NCEP atmospheric pressure and water vapor data. 6S models atmospheric scattering and gaseous absorption and corrects the optical TOA reflectance for it in order to acquire surface reflectance. Within this procedure, surface pressure data are used together with the GTopo30 DEM to adjust Rayleigh scattering to local conditions (Vermote et al. 1997, Masek et al. 2006). Rayleigh scattering describes the scattering of electromagnetic radiation on particles smaller than its wavelength (e.g. red sky sunset). For LEDAPS, an altered version of 6S is implemented, which was introduced by Kotchenova et al. (2006) (Vermote & Saleous 2007).

2.3 Radiometric Normalization

When combining several images to reduce overall cloud cover, their radiometric properties must be as similar as possible. All images in consideration should therefore be seasonally as close together as possible to reduce phenological variability, which strongly alters surface reflectance of vegetation. Yet, in several cases, temporal coverage of land surface reflectance was chosen over radiometric similarity.

Other causes for spectral variability are cloud cover, cloud shadow obstruction, change of land use/land cover, phenological variations and uncorrected atmospheric alterations. Due to the nonlinearity of these impacts, radiometric normalization between images should not be performed with a linear approach. In order to detect change between two image acquisitions, a regularized iteratively reweighted multivariate change detection (IR-MAD) (Nielsen 2007) was performed. IR-MAD is insensitive to linear change like gain and offset (histogram stretch), and most atmospheric correction schemes, and therefore, it can reliably detect true nontrivial change in multispectral data. Once pixels with least change have been determined, they can be used for radiometrically normalizing the images. This is described in detail by Canty & Nielsen (2008). Both routines are implemented within the iMAD software, whose open-source Python code was obtained via the personal homepage of Morton J. Canty (2012). An exemplary visualization of the effect of radiometric normalization can be seen in **Figure 2**.

As master reference for the normalization, the image acquisitions from May 12 1989, May 18 1994, May 23 1996 and March 26 2001 were chosen for each mosaic. The choice was based on percentage of cloud coverage and overall image quality mainly depending on unmasked cloud shadow, haze and thin cirrus clouds.

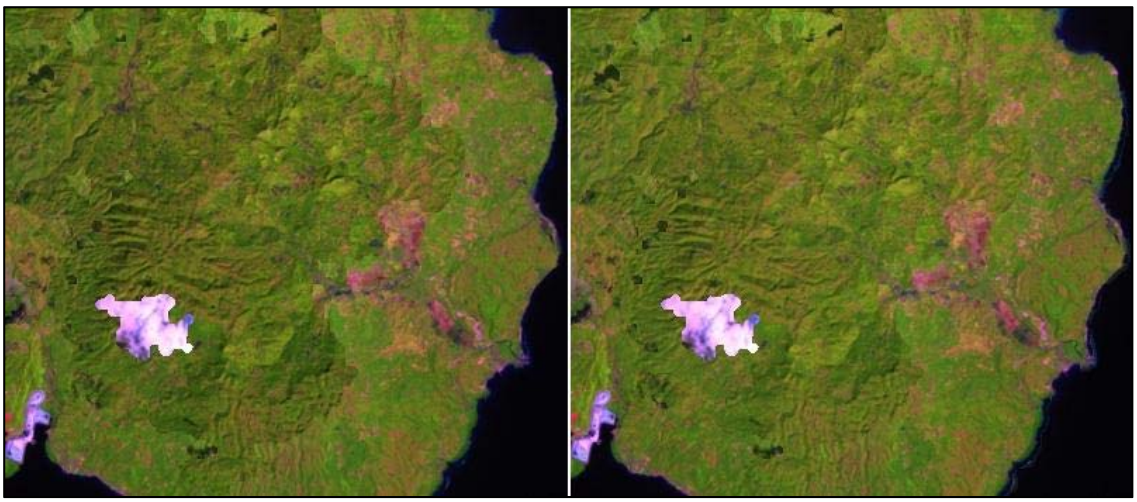

Figure 2. Effect of radiometric normalization on the quality of a stitched image
Left uncorrected, right corrected (5-4-3 color composite).

2.4 Cloud and Shadow Masking

The LEDAPS software incorporates the Automated Cloud Cover Assessment (ACCA) algorithm as described by Irish et al. (2006) as well as an internal surface reflectance based mask (SRBM). ACCA is the standard algorithm used by the Landsat Project Science Office (LPSO) of NASA's Goddard Space Flight Center (GSFC) to estimate percentage of cloud cover in Landsat image to be recorded in the US archive. The algorithm uses the spectral bands 2 through 6 to apply 26 decisions/filters to delineate cloud cover. A detailed description of the algorithm's processing steps is given in the Landsat-7 Science Data Users Handbook (NASA 2011:132–143). As reported by Vermote & Justice (2010:21), ACCA outperforms SRBM in terms of commission but is more prone to omission error. In this study, ACCA was found to drastically overestimate cloud cover; wherefore, it was excluded from further investigations.

For the purpose of this study, the output quality assessment (QA, integrating cloud cover and shadow obstruction) of LEDAPS was converted to a binary mask. The QA mask is delivered as 16-bit image layer and contains bit-packed quality flags. Converting these decimal values to binary format reveals unique combinations of binary quality flags as listed in **Table 1**. For instance, the decimal value 6 converts to binary value 110, which reveals that, read from right to left, this pixel contains valid data and was masked as cloud by the ACCA algorithm but not by the LEDAPS-internal cloud masking (as bit 8 is 0).

The masked (cloud and shadow obstructed) pixels were eroded to eliminate small pixel objects (noise). The remaining larger objects were dilated (expanded) to restore them to their original size including a buffer zone around masked areas. See **Figure 3** for a visualization of this procedure.

Table 1. Surface reflectance bit packed quality assessment (QA) flags (from documentation of LEDAPS model product [Masek et al. 2013])

bit	description
0	unused
1	valid data (1=yes)
2	ACCA cloud bit (1=cloudy)
3	unused
4	ACCA snow mask
5	land mask based on DEM (1=land)
6	Dark Dense Vegetation (DDV)
7	unused
8	internal cloud mask (1=cloudy)
9	cloud shadow
10	internal snow mask
11	land/water based on spectral test
12	adjacent cloud
13-15	unused

2.5 Terrain Correction

Sun illumination varies across a scene due to terrain-induced differences in orientation towards the sun, as well as inter-image differences caused by seasonal changes in sun elevation and aspect. This is most apparent in dark shadowed valleys and very light slopes in (or close to) zenith to the sun. In order to reduce this effect and normalize reflectance values originating from the same land cover, the C-Correction, as proposed by Teillet et al. (1982), was implemented. The approach was further extended to NDVI-thresholded correction, whereat correlations between surface reflectance values and sun illumination are evaluated separately for several NDVI-thresholded classes. The choice for C-Correction was based on the findings of Richter et al. (2009), who, in a comprehensive review, found this method to be superior to other prevalent approaches.

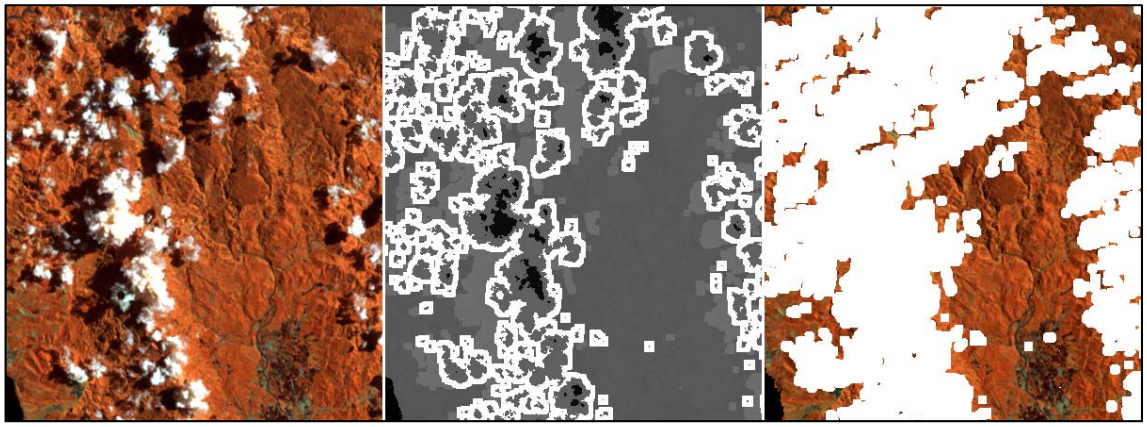

Figure 3. Performance of cloud masking

From left to right: original image (4-5-7 composite), LEDAPS quality assessment, fusion of manipulated mask and image. Error of commission was neglected in favor of low error of omission.

An exemplary visualization of the algorithm's performance can be seen in **Figure 4**. Although the method performs well on little to moderate slopes, shadow in terrain with steep slopes is missed, and reflectance of sun-zenith aligned slopes is further enhanced. This is primarily related to the lower 90-m geometrical resolution of the SRTM DEM and is at this moment inevitable. These errors are partly compensated for by a later performed Minimum Noise Fraction rotation (MNF).

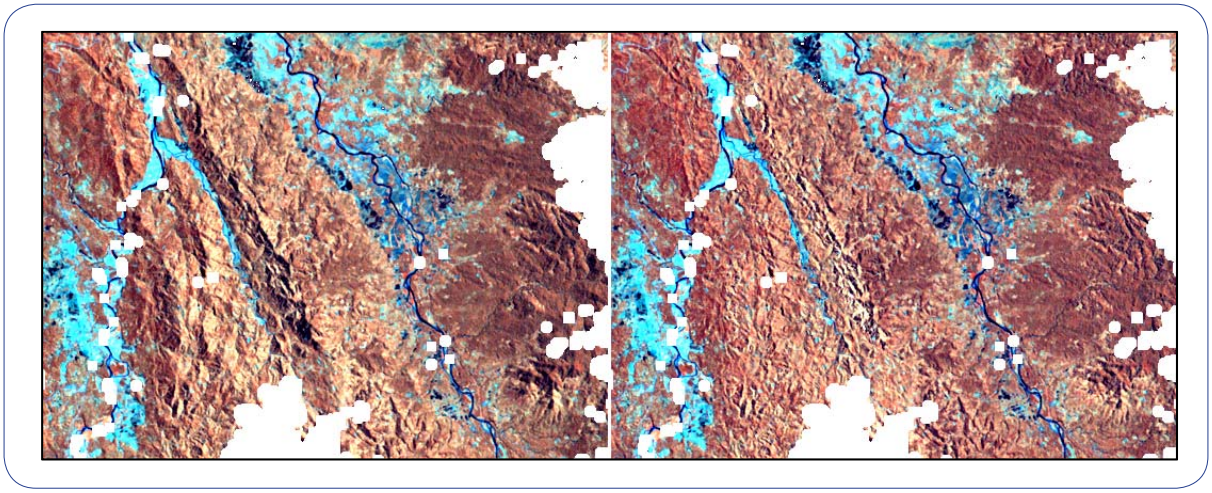

Figure 4. Image subset (4-5-7) showing the performance of the C-Correction for solar illumination

White pixels were masked for cloud and shadow obstruction.

3 Image Fusion

The master images used to start the fusion were the same images used for the radiometric normalization in Section 2.3. The stitching was then performed in a straight forward fashion, where if a pixel of the master or preliminary step fusion image is masked as cloud or cloud shadow and the corresponding pixel of the slave image is clear, this clear pixel is used to synthesize the new image. See **Figure 5** for an exemplary visualization of the performance.

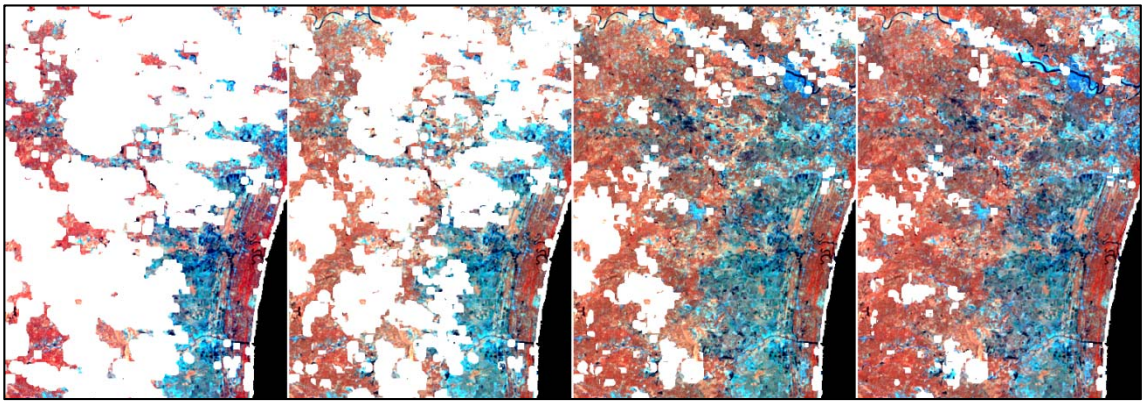

Figure 5. Subset of Eastern Leyte showing the performance of the cloud stitching, color composite 4-5-7 (NIR-SWIR1-SWIR2)

From left to right: master image acquired on Mar. 26, 2001, stepwise combination with image of date Dec. 4, 2000; Feb. 22, 2001; Apr. 11, 2001. Clouds and their shadows are masked white, whereas water is black.

4 Classification and Validation

As classifying algorithm, a Support Vector Machine (SVM) was chosen as implemented in the ENVI 5.0 software (refer to CHANG & LIN, 2001 and HSU et al., 2007 for algorithm descriptions). This choice was based on comparisons with other classifying algorithms. SVM showed to be least prone to errors originating from spectral inconsistency caused by insufficient radiometric normalization and cloud shadow masking. Training subsets were chosen across the island and validated using high-resolution Google Earth imagery.

For enhancing separability for choosing training subsets and the classifier, a Minimum Noise Fraction (MNF) Forward Transformation was performed for Landsat bands 1, 2, 3, 4, 5 and 7. The six resulting layers were then, after choosing representative samples of the required classes, supplied to the SVM routine. The MNF transformation separates between-band spectral correlation in multispectral data according to the Principal Component Analysis (PCA) principle and orders the resulting components by their signal-to-noise ratio (SNR) (Green et al. 1988:65ff.). Concerning the selection of training samples, this procedure was particularly beneficial as inter-image radiometric inconsistency was enhanced and could be sampled appropriately. Mentioning the insufficient illumination correction in mountainous areas, in some cases, this effect was found to be partly eliminated in the noisiest MNF components. Yet, this effect still introduced the largest error for the forest class.

Figure 6 displays the spectral variability in the used image channels for the most critical classes (forest, transition and palm) as boxplots.

For assessing the accuracy or quality of the classification, another set of test areas was chosen from ground truth acquired in July 2013 and comparison with Google Earth, and then checked against the classification of the area. The test samples were chosen in the Landsat image, as direct definition from ground truth polygons and the Google Earth image would introduce additional error due to the large difference of the acquisition dates. The results for each year are displayed in **Tables 2 to 5**.

Overall accuracy was found to be between 81 and 90%. The Kappa coefficients were 0.74, 0.87, 0.83 and 0.77 for the years 1989, 1993, 1995 and 2000, respectively. Largest errors are encountered by delineating forest. The Urban/Bare class was matched very well due to its strong contrast to the vegetated areas.

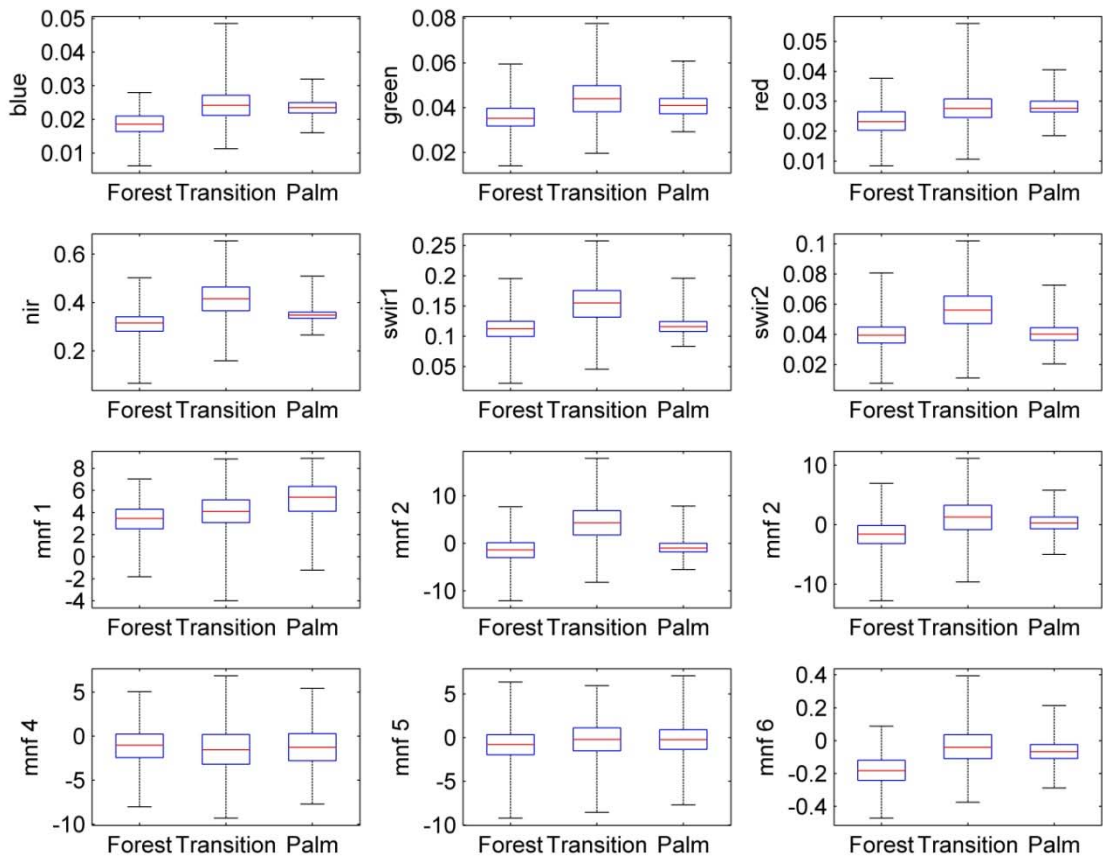

Figure 6. Spectral variability of forest, palm and transitional zone (mixed pixels) reflectance and MNF eigenvalues for selected subsets

The red line represents the mean value; the blue box delineates variance and the whiskers mark minimum and maximum values.

Table 2. 1989-1990 accuracy assessment

Class	Forest	Palm	Mix	Agri/Bare	Total	Commission
Forest	**348**	20	3	1	372	93.55
Palm	53	**565**	87	0	705	80.14
Mix	164	63	**551**	1	779	70.73
Agri	91	8	20	**664**	783	84.8
Total	656	656	661	666	**2639**	
Omission	53.05	86.13	83.36	99.7		**80.64**

Top-down: test samples vs. classification (omission or producer's accuracy); left-right: classification vs. test samples (commission or user's accuracy).

Table 3. 1993-1994 accuracy assessment

Class	Forest	Palm	Mix	Agri/Bare	Total	Commission
Forest	**580**	16	28	0	624	92.95
Palm	66	**602**	18	2	688	87.5
Mix	51	74	**610**	2	737	82.77
Agri	0	1	2	**647**	650	99.54
Total	697	693	658	651	**2699**	
Omission	83.21	86.87	92.71	99.39		**90.37**

Table 4. 1995-1996 accuracy assessment

Class	Forest	Palm	Mix	Agri/Bare	Total	Commission
Forest	**528**	38	44	0	610	86.56
Palm	134	**631**	22	1	788	80.08
Mix	35	13	**555**	0	603	92.04
Agri	8	3	40	**666**	717	92.89
Total	705	685	661	667	**2718**	
Omission	74.89	92.12	83.96	99.85		**87.56**

Table 5. 2000-2001 accuracy assessment

Class	Forest	Palm	Mix	Agri/Bare	Total	Commission
Forest	**581**	65	72	6	724	80.25
Palm	41	**541**	10	3	595	90.92
Mix	108	130	**553**	1	792	69.82
Agri	11	8	54	**737**	810	90.99
Total	741	744	689	747	**2921**	
Omission	78.41	72.72	80.26	98.66		**82.57**

5 Change Detection

5.1 Preliminary Agriculture Mask

For detecting true change in land cover/use, areas of agricultural use need to be identified. Due to their strong phenological variation and change to bare soil across seasons, areas of true change can easily be overestimated. With the aim of reducing this error, the NDVI was derived for each image acquisition of one time frame (year), maximum, minimum and their difference calculated and thresholded to identify areas that have undergone large changes in NDVI following conditions.

$$NDVI_{diff} > 0.1;\ NDVI_{min} < 0.6,$$

where $NDVI_{diff}$ is the difference of maximum and minimum NDVI value for each pixel, along the specified time frame, and $NDVI_{min}$ is the minimum value. Thresholding was particularly necessary for excluding larger forest areas that expressed large NDVI changes across images due to insufficient correction or masking of atmospheric effects. See **Figure 7** for a visualization of the method's performance.

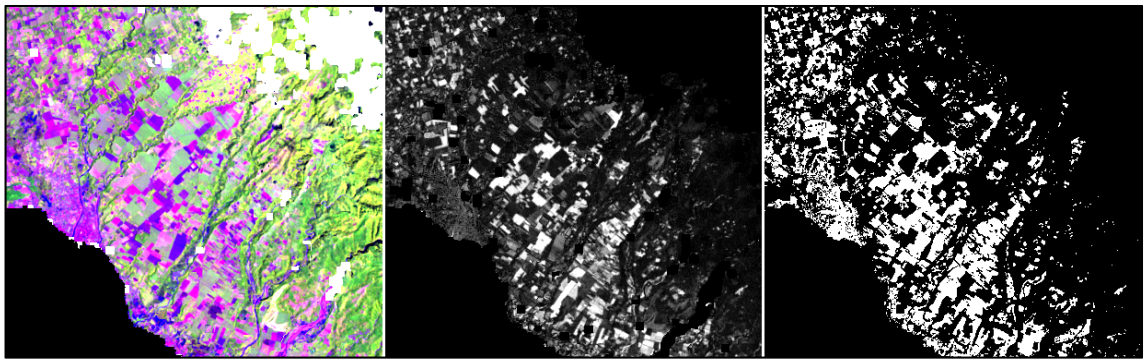

Figure 7. Masking of agricultural area
From left to right: 5-4-3 composite image subset, differential NDVI, thresholded mask.

5.2 Post-Classification Change Detection

Change is detected in the manner of cross-comparing all classification results of the time frame. If one pixel is classified as forest or mix of natural trees and palm trees, but is classified as agriculture or bare soil in the following time step, it is marked as deforested. This condition then only holds true if the pixel was not classified as bare soil or agriculture in any time step before the forest classification. Lastly, all pixels identified as deforested are cross-checked with the preliminary agriculture mask discussed in Section 5.1 and are excluded if they have been identified as agriculture.

Table 6. Area statistics of classification results in hectare

[ha]	1989-1990	1993-1994	1995-1996	2000-2001	Fusion
Forest	50713.02	106204.32	111518.46	110662.65	146829.15
Mix	106168.05	100042.38	123214.41	134953.65	139180.68
Palm	50110.38	70576.65	122552.73	90574.47	87022.98
Agriculture	109126.35	74288.43	190131.12	60366.42	213587.55
Bare/Urban	217546.47	77249.70	53858.34	156424.23	53850.87
Masked	188020.08	274581.27	99653.85	141548.40	15324.30
Defo1	0.00	5168.34	10436.13	13091.49	28502.37
Defo2	0.00	13668.57	10422.72	14166.45	37484.01

Defo1 and Defo2 are Deforestation of Forest and Mix, respectively.

Table 7. Area statistics of classification results in percent

[%]	1989-1990	1993-1994	1995-1996	2000-2001	Fusion
Forest	7.03	14.71	15.45	15.33	20.34
Mix	14.71	13.86	17.07	18.70	19.28
Palm	6.94	9.78	16.98	12.55	12.06
Agriculture	15.12	10.29	26.34	8.36	29.59
Bare/Urban	30.14	10.70	7.46	21.67	7.46
Masked	26.05	38.04	13.81	19.61	2.12
Defo1	0.00	0.72	1.45	1.81	3.95
Defo2	0.00	1.89	1.44	1.96	5.19

6 Discussion

Forest cover and palm land use were reliably well classified within the scope of this study. Yet, within the processing chain, several steps can be improved to further increase the quality of the final product. Some of the flaws will be described in the following to outline potential for further investigations. For this, not the theoretical basis of particular algorithms implemented elsewhere is questioned nor validated, as this was out of scope of this study. Rather, focus is put on reliability of the processing chain and applicability to succeeding studies.

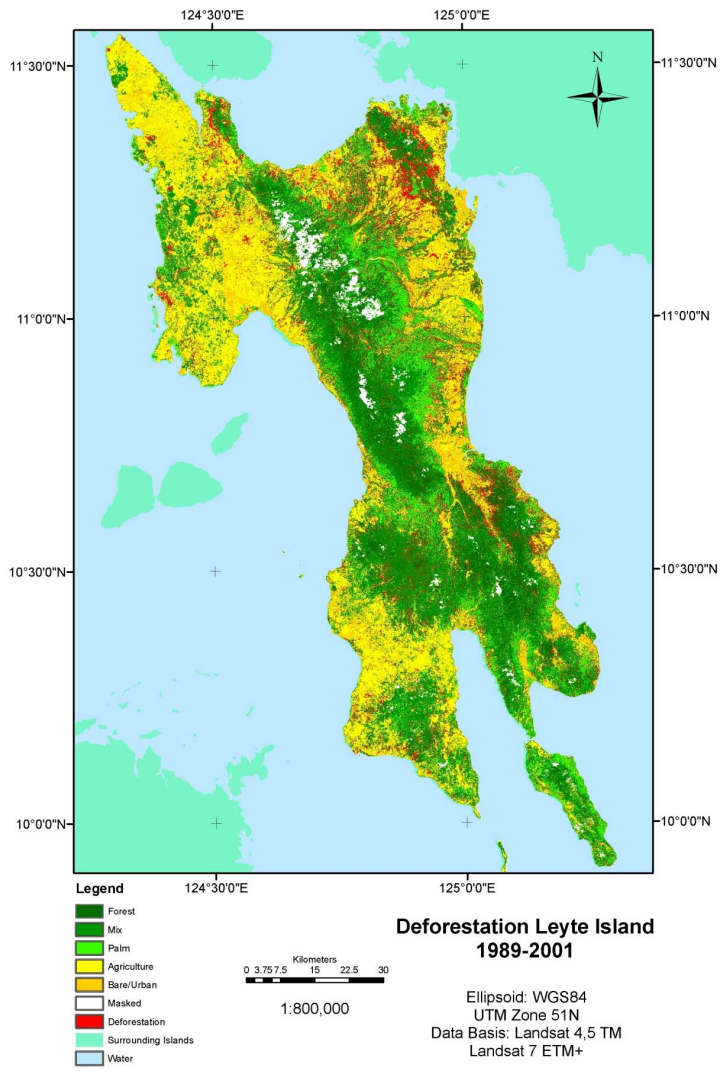

Figure 8. Land cover/use and deforestation map of Leyte Island for the years 1989 to 2001

6.1 Cloud and Cloud Shadow Masking

The algorithm was found to overestimate cloud shadow in various situations, particularly mistaking dark bare soil and riverbeds for shadow. Masked clouds were not precisely outlined in many cases (over- and underestimation), which demanded further editing of the mask through eroding and dilating. Cloud and cloud shadow obstruction of the final product could be decreased by implementing a more precise and therefore less generous masking, declaring a larger area as free of clouds and shadow. An implementation of a refined procedure is considered rather time consuming, as the applicability to other atmospheric and seasonal situations needs to be comprehensively evaluated. The LEDAPS QA mask was found to omit several bit combinations. Bits 9 (cloud shadow) and 12 (adjacent cloud) never exist together, which complicates manipulations on singular bitmasks. An image object segmentation approach is suggested for further refining. A more critical difficulty presents the insufficient masking of occasionally encountered large cloud shadows. This case is most noticeable in areas of mixed trees or palm plantations, which are accordingly mistaken for forest.

6.2 Radiometric Normalization

Although the MAD procedure is significantly enhancing the quality of the final product, visual inspection revealed room for improvement. Other methods are suggested in literature, which have been shown to perform better. Refer to Helmer & Ruefenacht (2007) for a comparative study on different approaches. Here, a regression tree method is suggested, which can be implemented in open source versions. Yet, documentation on the application of this code (written in R) is poorly documented and requires further research beyond this study. However, by carefully selecting training subsets on the MNF transformed image, poorly normalized image mosaic patches can be accounted for. Extreme cases of insufficient normalization were only found with images of extreme cloud obstruction, incapacitating the MAD routine of finding an adequate set of unchanged samples for radiometric correlation computations. This case could be accounted for by redesigning the MAD and radiometric normalization algorithms to more efficiently use available memory. Currently, the whole image is read at once, therefore only allowing smaller subset processing. Implementing band-wise array, computing in combination with water masking, would enable sample selection across the whole island for specifying the linear regression.

Further research is also suggested to determine the effect of image acquisition date and therefore the phenological variability on the quality of normalization.

6.3 Classification and Validation

The SVM method has been proven to be very robust and flexible compared to other approaches and is gaining wide acceptance in the field of research, see for e.g. Townshend et al. (2012:13), who used this method to create global forest maps with Landsat data. In this study, SVM was also observed to be less mistaken by spectral changes related to unmasked shadow.

The largest uncertainty when classifying images lies in the selection of training samples. Reference satellite data, with beneficial resolution, spectral, temporal and radiometric, might not be available. Ground truth campaigns are time consuming but necessary to gain comprehensive understanding of land cover. Yet, cross-comparison with images acquired in different years is to be performed with caution, as essential change might occur in small time steps.

Separability of forest, mix and palm was observed to strongly depend on SWIR reflectance, which is closely related to moisture. The effect of seasonal moisture changes on separability of these classes and is yet to be assessed in a wider scope. This might, if changes are little, allow for selecting images across the whole year for mosaicking.

6.4 Change Detection

As inherent to post-classification change detection, the accuracy of the result is strongly dependent on the accuracy of the single classification results and never better than those. Yet, in the scope of this study, it was assumed to offer the best compromise. Methods like Change Vector Analysis (CVA, Malila 1980) or MAD (Canty & Nielsen 2008) are well suited for detecting spectral change, yet the nature of change remains concealed. Moreover, change can have numerous causes, with unmasked cloud shadow and changing illumination in steep mountainous areas being the most conceiving. In this study, change was therefore limited to the most distinctive case, where a pixel is marked as deforested if it was forest or mix, and then is bare soil or agriculture. The spectral signatures of these classes are very well separable and unlikely mistaken by the classifier, even though the actual bare soil area might be much smaller than the pixel. The largest error in this procedure is introduced by the ambiguity of the agriculture class, which frequently undergoes these changes. The accuracy of identified change is therefore strongly dependent on the temporal resolution of the pixel. More samples of each pixel are available per year and make the identified change less ambiguous.

Accordingly, it is necessary to observe that the accuracy of the identified deforestation varies across the image, depending on the sampling of each pixel. This is dependent on the number of cloud-free acquisitions per time step and the time step itself. Later observed change is more accurate, as more cross-checks with earlier images can be incorporated.

7 Conclusion

The pursued procedure of integrating several Landsat images to classify mosaicked images and then detecting deforestation changes from 1989 to 2001 was found to be very reliable in encountering difficulties as cloud cover and spectral variability gave very satisfactory robust classification results. Calibration, atmospheric correction, radiometric normalization and cloud masking enabled the creation of homogenous image mosaics fused together of images acquired on various dates and conditions. Throughout this paper, several indications about further improving the workflow are given. The most striking ones are radiometric normalization and a more complex inter-dependency change detection approach.

This approach will further improve if more images are incorporated, particularly in the case of change detection, as this is specified by cross-checking with different image acquisitions. The biggest limiting factor in this analysis is cloud and cloud shadow obstruction, which strongly limit the study area. The established workflow enables the analyst to easily expand the scope of analyzed image frames through the use of primarily automatized procedures.

With the perspective of installing a nationwide satellite MRV system, this study is seen as an important framework for tracking medium geometric resolution land cover and land use changes, which can easily be extended to different areas and time frames as long as a sufficient number of images is available. This is not always ensured due to very high percentage of cloud obstruction and Landsat technical problems like inconsistent spatial coverage for Landsat 7. Use of different datasets, like Synthetic Aperture Radar (SAR) and higher geometric resolution optical images, is strongly recommended to enhance temporal accuracy and small-scale detail of deforestation mapping.

References

Canty, M.J. (2012): Personal Homepage. <mcanty.homepage.t-online.de> (Status: 2012-08-08) (Access: 2013-05-15).

Chang, C.-C. & C.-J- Lin (2001): LIBSVM: a Library for Support Vector Machines. National Taiwan University, Department of Computer Science & Information Engineering NTU CSIE online. <http://www.csie.ntu.edu.tw/~cjlin/papers/csvm. pdf>.

DfS Deutsche Forstservice GmbH (2013): "Forest Carbon Baseline Study Leyte. Final draft report. GIZ German Technical Cooperation with the Philippines. Climate Relevant Forest Policy and Piloting of REDD."

Estomata, M.T. (2013A): "ALOS PALSAR 25-meter Mosaic Step-by-step Manual on Extraction of Forest Cover and Change Detection Analysis – A Manual for Users". Deutsche Gesellschaft für Internationale Zusammenarbeit (GIZ) GmbH.

———. (2013B): "Support to Processing of Remote Sensing Data for the Establishment of a Pilot MRV System for REDD+ on Leyte Island". GIZ German Technical Cooperation with the Philippines.

Green, A.A., M. Berman, P. Switzer & M.D. Craig (1988): A Transformation for Ordering Multispectral Data in Terms of Image Quality with Implications for Noise Removal. –IEEE Transactions on Geoscience and Remote Sensing 26, 1, 65-74.

GIZ (2012): Support of processing Remote Sensing Data for the Establishment of a pilot MRV System for REDD+ on Leyte Island. Terms of Reference. Gesellschaft für Internationale Zusammenarbeit GIZ GmbH.

Helmer, E.H. & B. Ruefenacht (2007): A Comparison of radiometric Normalization Methods when filling Cloud Gaps in Landsat Imagery. –Canadian Journal of Remote Sensing 33, 4, 325-340.

Hsu, C.-W., C.-C. Chang & C.-J. Lin (2007): A practical Guide to Support Vector Classification. National Taiwan University, Department of Computer Science & Information Engineering NTU CSIE online. <http://ntu.csie.ntu.edu.tw/~cjlin/ papers/guide/guide.pdf.

Irish, R.R., J.L. Barker, S.N. Goward & T. Arvidson (2006): Characterization of the Landsat-7 ETM+ Automated Cloud-Cover Assessment (ACCA) Algorithm. –Photogrammetric Engineering & Remote Sensing 72, 10, 1179-1188.

Kaufman, Y.J., A.E. Wald, L.A. Remer, B.-C. Gao, R.-R. Li & L. Flynn (1997): The MODIS 2.1 µm Channel – Correlation with Visible Reflectance for Use in Remote Sensing of Aerosol. –IEEE Transactions on Geoscience and Remote Sensing 35, 5, 1286-1298.

Kistler, R., E. Kalnay, W. Collins, S. Saha, G. White, J. Woollen, M. Chelliah, W. Ebisuzaki, M. Kanamitsu, V. Kousky, H. VanDeDool, R. Jenne & M. Fiorino (2001): The NCEP-NCAR 50-Year Reanalysis: Monthly Means CD-ROM and Documentation. –Bulletin of the American Meteorological Society 82, 2, 247-268.

Kotchenova, S.Y., E.F. Vermote, R. Matarrese & F. Klemm (2006): Validation of a new Vector Version of the 6S radiative Transfer Code for atmospheric Correction of MODIS Data: Part I – Path Radiance. – Applied Optics 45, 26, 6762-6774.

Malila (1980): Change Vector Analysis: an Approach detecting Forest Changes with Landsat. –Proceedings of the 6th International Symposium on Machine Processing of Remotely Sensed Data, 326-335.

Masek, J.G., E.F. Vermote, N. Saleous, R. Wolfe, F.G. Hall, F. Huemmrich, F. Gao, J. Kutler, and T.K. Lim (2006): A Landsat Surface Reflectance Dataset for North America, 1990-2000. –IEEE Geoscience and Remote Sensing Letters 3, 1, 68-72.

Masek, J.G., E.F. Vermote, N. Saleous, R. Wolfe, F.G. Hall, F. Huemmrich, F. Gao, J. Kutler, and T.K. Lim (2013): LEDAPS Calibration, Reflectance, Atmospheric Correction Preprocessing Code, Version 2. Model product. Available online from Oak Ridge National Laboratory Distributed Active Archive Center, Oak Ridge, Tennessee, U.S.A. <http://dx.doi.org/10.3334/ ORNLDAAC/1146>.

McPeters, R.D., P.K. Bhartia, A.J. Krueger, J.R. Herman, C.G. Wellemeyer, C.J. Seftor, G. Jaross, O. Torres, L. Moy, G. Labow, W. Byerly, S.L. Taylor, T. Swissler & R.P. Cebula (1998): Earth Probe Total Ozone Mapping Spectrometer (TOMS) Data Products User's Guide. NASA Technical Publication 1998-206895. Greenbelt, Goddard Space Flight Center.

NASA (2011): Landsat 7 Science Data Users Handbook. <http://landsathandbook. gsfc.nasa.gov>.

NCEP/NCAR (2001): NCEP/NCAR Global Reanalysis Products, 1948-continuing. National Oceanic and Atmospheric Administration (NOAA), National Weather Service (NWS), National Centers for Environmental Prediction (NCEP). –Research Data Archive at the National Center for Atmospheric Research (NCAR), Computational and Information Systems Laboratory <http://rda.ucar.edu/ datasets/ ds090.0>.

Nielsen, A.A. (2007): The Regularized Iteratively Reweighted MAD Method for Change Detection in Multi- and Hyperspectral Data. –IEEE Transactions on Image Processing 16, 2, 463-478.

Richter, R., T. Kellenberger & H. Kaufmann (2009): Comparison of Topographic Correction Methods. –Remote Sensing 1, 184-196.

Seifert-Granzin, J. (2013): Conceptual approach to REDD+ MRV in the Philippines - An Overview. Updated Version 2.0. Mesa consult.

Teillet, P.M., B. Guindon & D.G. Goodenough (1982): On the Slope-Aspect Correction of multispectral Scanner Data. –Canadian Journal of Remote Sensing 8, 84-106.

Townshend, J.R., J.G. Masek, C. Huang, E.F. Vermote, F. Gao, S. Channan, J.O. Sexton, M. Feng, R. Narasimhan, D. Kim, K. Song, D. Song, X.-P. Song, P. Noojipady, B. Tan, M.C. Hansen, M. Li & R.E. Wolfe (2012): Global Characterization of Forest Cover using Landsat Data: Opportunities and Challenges. –International Journal of Digital Earth, 1-25.

USGS EROS (2012): GTOPO30. Official homepage. United States Geological Survey, Earth Resources Observation and Science. <http://eros.usgs.gov/#/Find_Data/ Products_and_Data_Available/ gtopo30_info>. (Status: 2012-09-27) (Access: 2013-06-06).

Vermote, E.F. & N. Saleous (2007): LEDAPS Surface Reflectance Product Description. Version 2. <http:// ledaps.nascom.nasa.gov>.

Vermote, E. & C. Justice (2010): A Surface Reflectance standard Product from LDCM and supporting Activities. June 2010 Update. USGS online presence <http://landsat.usgs.gov/documents/> (status: 28.12.2010) (access: 14.08.2013).

Vermote, E.F., N. El Saleous, C.O. Justice, Y.J. Kaufman, J.L. Privette, L. Remer, J.C. Roger & D. Tantre (1997): Atmospheric Correction of visible to middle-infrared EOS-MODIS data over land surfaces: Background, operational algorithm and validation. –Journal of Geophysical Research 102, 17131-17141.

Annexes

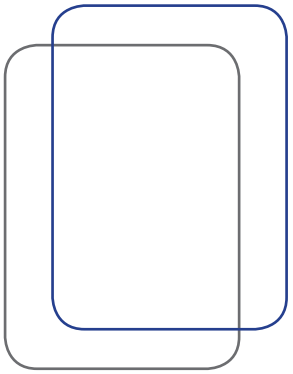

Annexes

Tab. 1: List of integrated images. Separating lines delineate the four produced image mosaics. One full island coverage per acquisition date was, if possible, produced from two single images. Master acquisitions for radiometric normalization and image fusion are further highlighted in bold letters.

Acquisition Date	Image ID	Sensor	coverage
19890325	LT41130531989084XXX01	LS4-TM	South
19890410	LT41130521989100XXX02	LS4-TM	North
19890426	LT41130531989116XXX01	LS4-TM	South
19890512	**LT41130521989132XXX02**	**LS4-TM**	**North**
19890512	**LT41130531989132XXX02**	**LS4-TM**	**South**
19890528	LT41130521989148XXX02	LS4-TM	North
19890528	LT41130521989148XXX02	LS4-TM	South
19890613	LT41130521989164XXX02	LS4-TM	North
19890613	LT41130531989164XXX02	LS4-TM	South
19901225	LT41130521990359XXX01	LS4-TM	North
19901225	LT41130531990359XXX03	LS4-TM	South
19930616	LT51130521993167CLT00	LS5-TM	North
19930616	LT51130531993167CLT00	LS5-TM	South
19930819	LT51130521993231CLT00	LS5-TM	North
19930819	LT51130531993231CLT00	LS5-TM	South
19940518	**LT51130521994138CLT00**	**LS5-TM**	**North**
19940518	**LT51130531994138CLT00**	**LS5-TM**	**South**
19940721	LT51130521994202CLT00	LS5-TM	North
19940721	LT51130531994202CLT00	LS5-TM	South
19950505	LT51130521995125DKI00	LS5-TM	North
19950505	LT51130531995125DKI00	LS5-TM	South
19950521	LT51130521995141DKI00	LS5-TM	North
19950521	LT51130531995141DKI00	LS5-TM	South
19960421	LT51130521996112CLT00	LS5-TM	North
19960421	LT51130531996112CLT00	LS5-TM	South
19960507	LT51130521996128CLT00	LS5-TM	North
19960507	LT51130531996128CLT00	LS5-TM	South
19960523	**LT51130521996144CLT00**	**LS5-TM**	**North**
19960523	**LT51130531996144CLT00**	**LS5-TM**	**South**
20001204	LE71130522000339EDC00	LS7-ETM+	North
20001204	LE71130532000339EDC00	LS7-ETM+	South
20010222	LE71130522001053EDC00	LS7-ETM+	North
20010222	LE71130532001053EDC00	LS7-ETM+	South
20010326	**LE71130522001085SGS00**	**LS7-ETM+**	**North**
20010326	**LE71130532001085SGS00**	**LS7-ETM+**	**South**
20010411	LE71130522001101DKI00	LS7-ETM+	North
20010411	LE71130532001101SGS00	LS7-ETM+	South

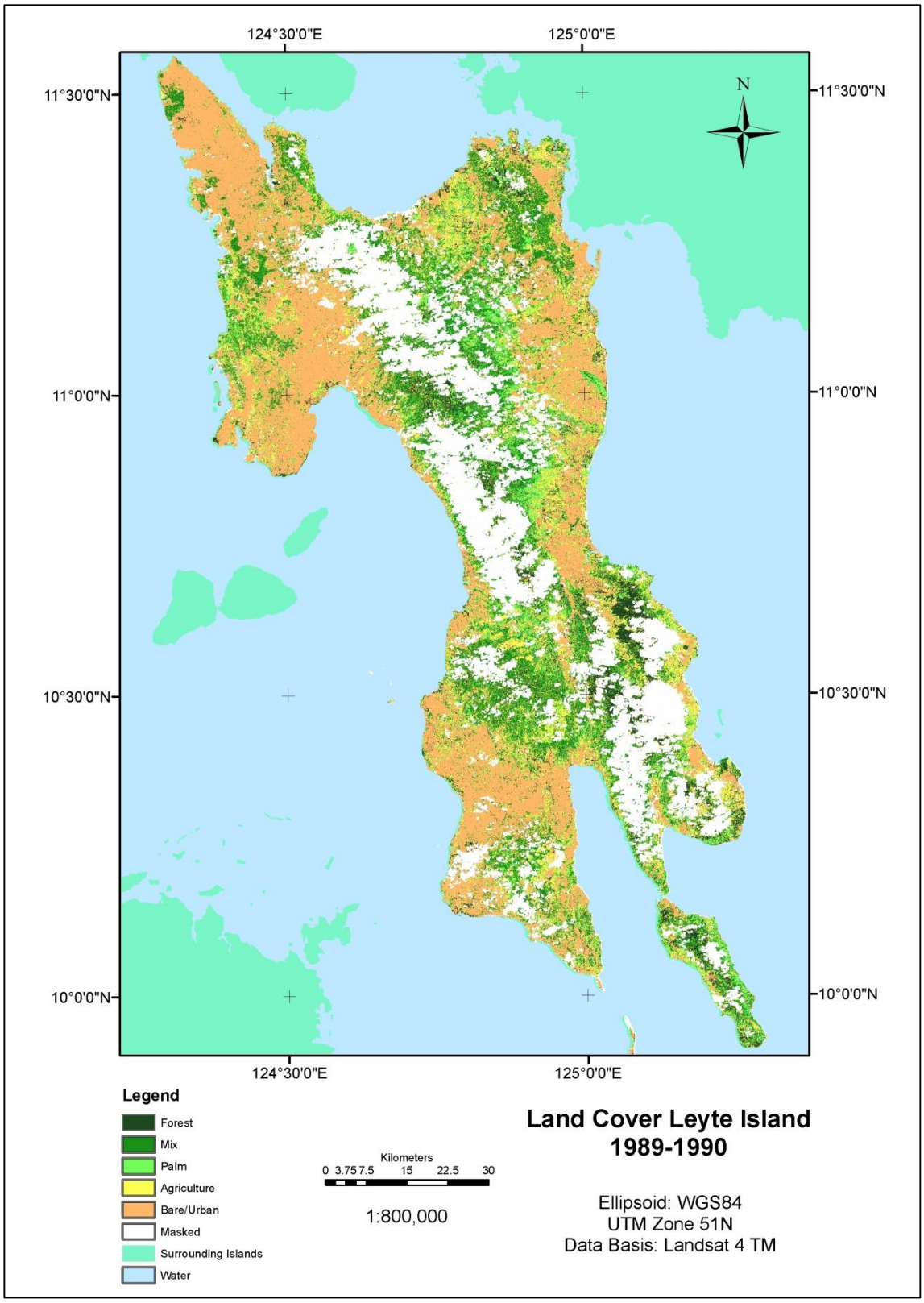

Fig. 1: Classification result of 1989-1990 image mosaic.

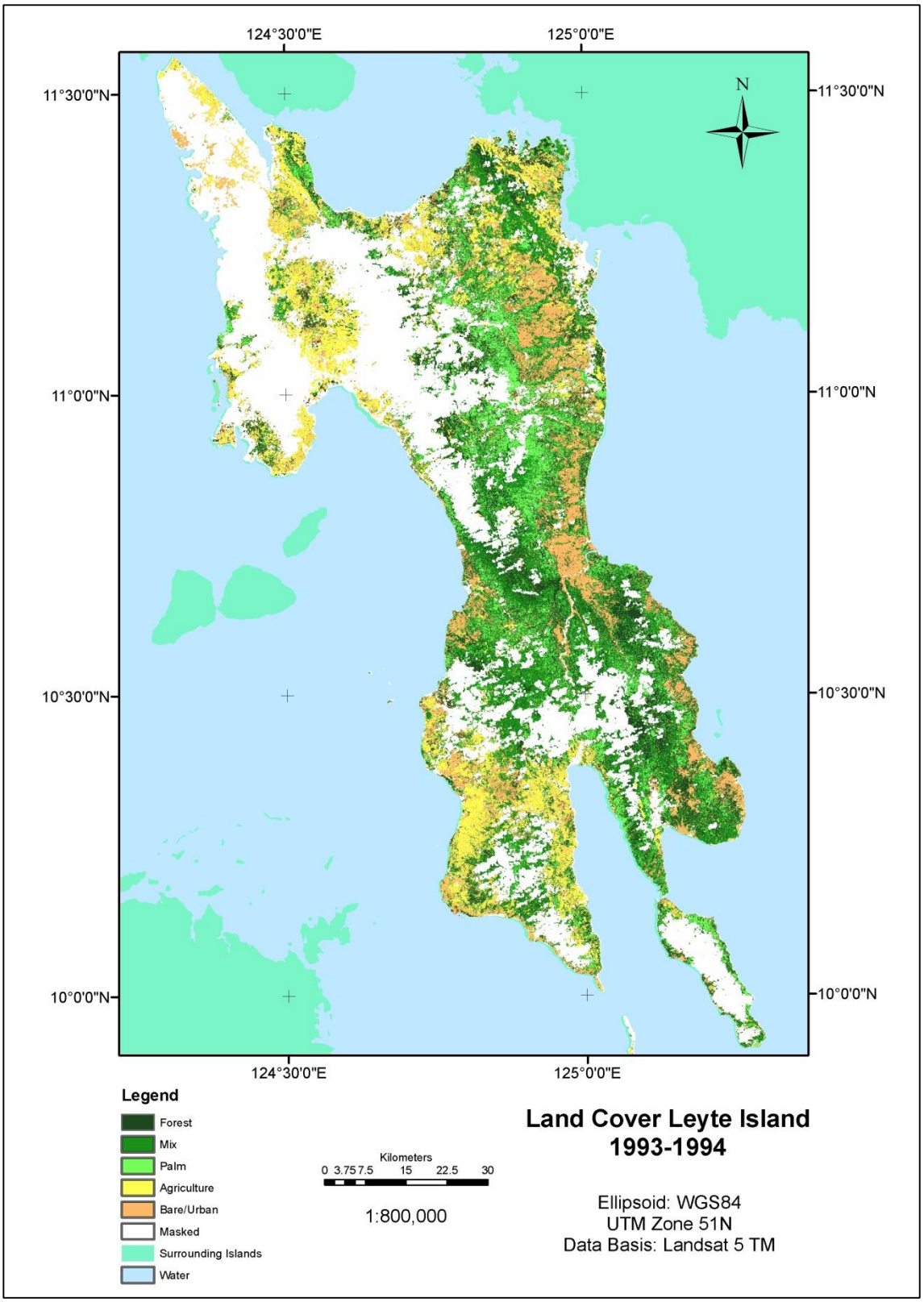

Fig. 2: Classification result of 1993-1994 image mosaic.

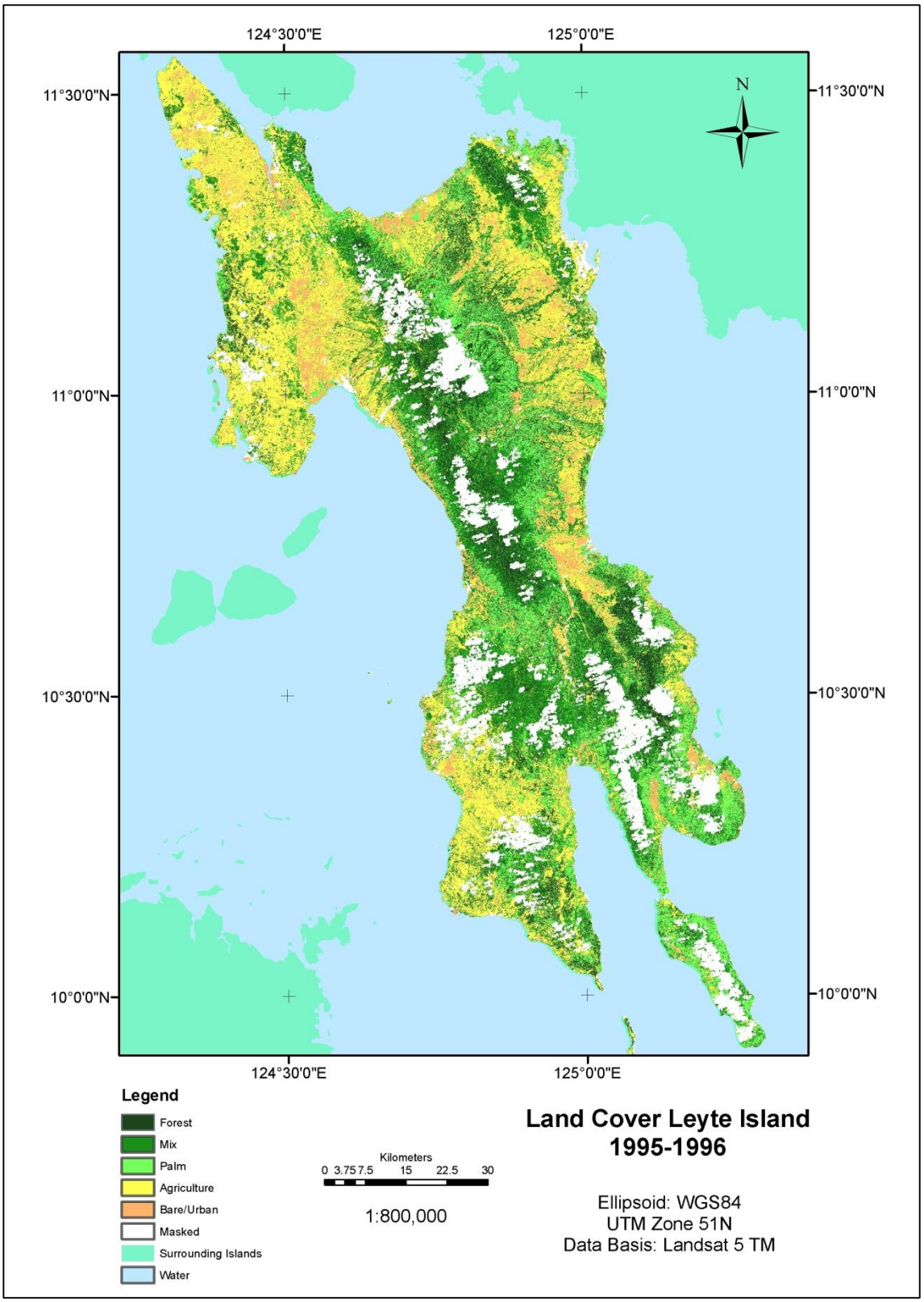

Fig. 3: Classification result of 1995-1996 image mosaic.

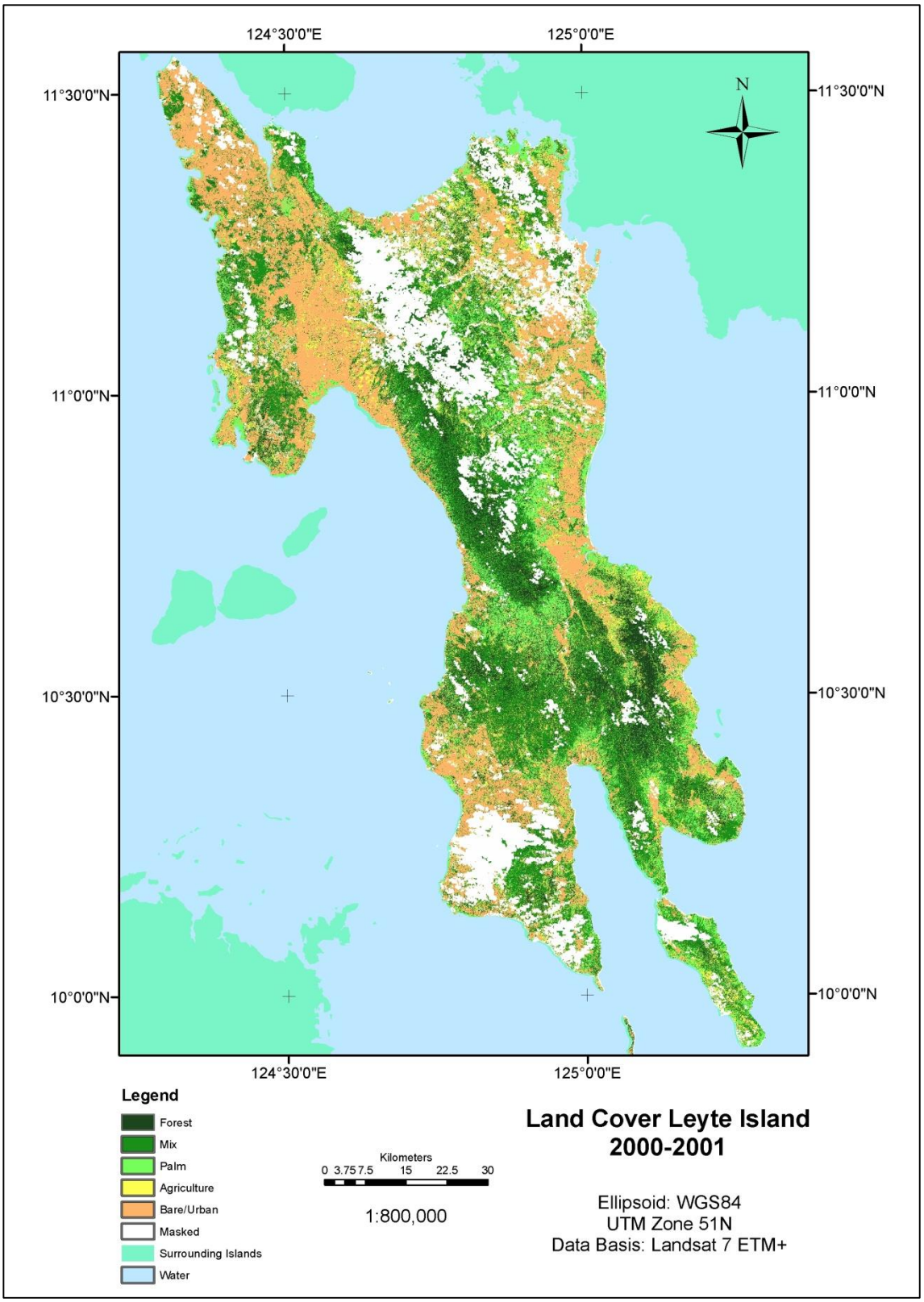

Fig. 4: Classification result of 2000-2001 image mosaic.